UC Davis
UC Davis Previously Published Works

Title

Decision and response monitoring during working memory are sequentially represented in the human insula.

Permalink

Journal

Authors

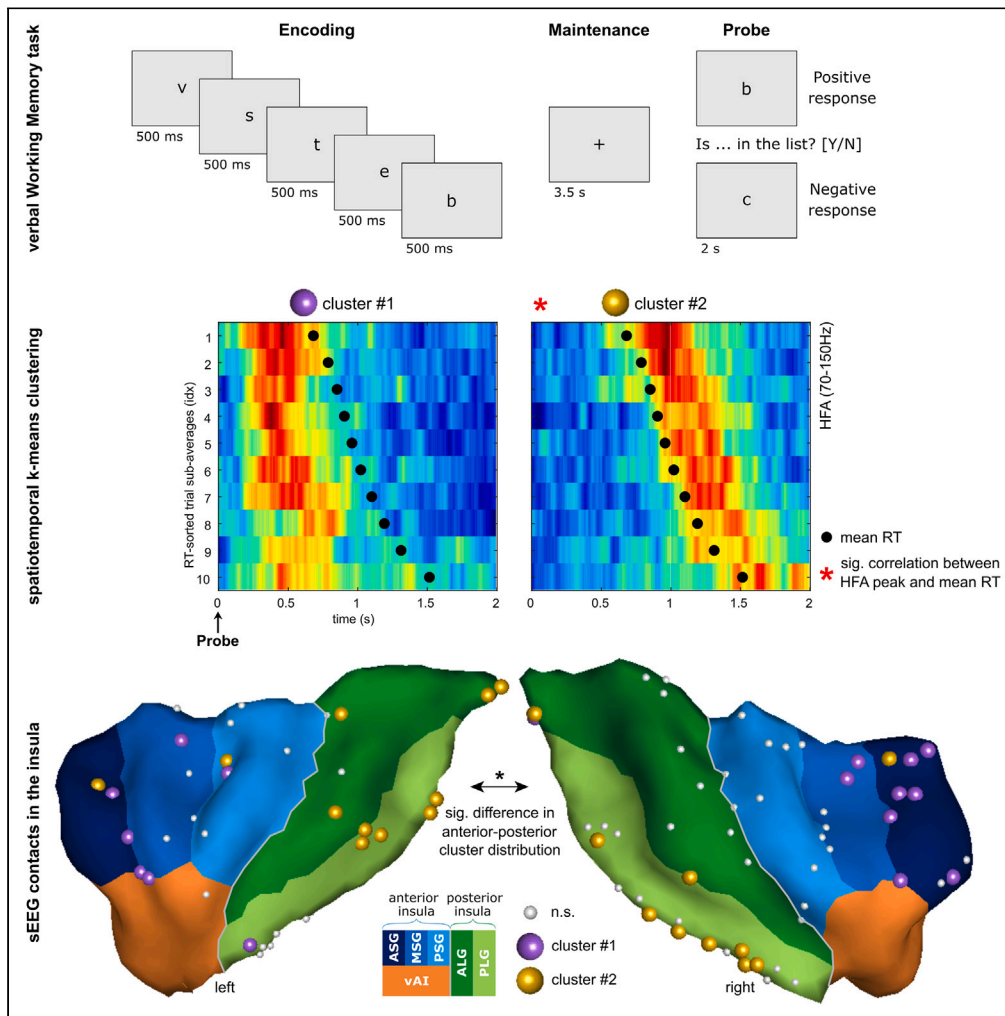Llorens, Anaïs
Bellier, Ludovic
Blenkmann, Alejandro
et al.

Publication Date

DOI

Peer reviewed

Article

Decision and response monitoring during working memory are sequentially represented in the human insula

Anaïs Llorens, Ludovic Bellier, Alejandro O. Blenkmann, ..., Tor Endestad, Anne-Kristin Solbakk, Robert T. Knight

anaisllorens@hotmail.com

Highlights

We defined a functional anteroposterior gradient of the insula during working memory

The anterior insula is involved in decision making

The posterior insula is involved in sensorimotor responses monitoring

Article

Decision and response monitoring during working memory are sequentially represented in the human insula

Anaïs Llorens,[1,2,3,10,12,*] Ludovic Bellier,[1,10] Alejandro O. Blenkmann,[6,7] Jugoslav Ivanovic,[4] Pål G. Larsson,[4] Jack J. Lin,[5] Tor Endestad,[6,7,8] Anne-Kristin Solbakk,[4,6,7,8,11] and Robert T. Knight[1,9,11]

SUMMARY

Emerging research supports a role of the insula in human cognition. Here, we used intracranial EEG to investigate the spatiotemporal dynamics in the insula during a verbal working memory (vWM) task. We found robust effects for theta, beta, and high frequency activity (HFA) during probe presentation requiring a decision. Theta band activity showed differential involvement across left and right insulae while sequential HFA modulations were observed along the anteroposterior axis. HFA in anterior insula tracked decision making and subsequent HFA was observed in posterior insula after the behavioral response. Our results provide electrophysiological evidence of engagement of different insula subregions in both decision-making and response monitoring during vWM and expand our knowledge of the role of the insula in complex human behavior.

INTRODUCTION

Interest in the human insula has increased commensurate with the development of improved methods to study this structure.[1,2] The insula is located deep within the lateral sulcus of the brain.[3] It is divided by the central insular sulcus into anterior (three short gyri and one accessory gyrus) and posterior parts (two long gyri), and outlined by the circular sulcus.[4,5] The insula shares bidirectional connections with multiple regions of the neocortex, including prefrontal cortex (PFC), anterior cingulate cortex (ACC), supplementary motor area (SMA), parietal, occipital, and temporal cortices. It also connects with medial temporal and adjacent limbic structures[6,7] as well as with the basal ganglia.[8,9] This extensive connectivity places the insula as an ideal neuroanatomical hub supporting numerous cognitive and limbic functions[1,10–12] with overlapping and distinct roles played by its different subregions and across both hemispheres.[13–15] Some reports note differential inter-hemispheric involvement, with the left insula preferentially observed in response inhibition and language processing and the right insula in error prediction, error detection, memory, and attention.[6,16–22]

Cytoarchitectural, imaging, and modeling studies report a spatial posterior-to-anterior gradient linked to a progressive integration of complex behaviors including top-down control.[17,23–26] Broadly, the insula can be divided into three anatomical subregions which play distinct functional roles in human cognition, albeit with some overlap.[21,27] The posterior insula is preferentially connected to parietal, occipital, and temporal association cortices and is involved in interoceptive experiences, emotional and affective states, somatosensory, viscerosensory, and sensorimotor functions, speech production, and primary and association auditory responses.[5,17,23,24,28–32] The anterior insular cortex (AIC), composed of a ventral and a dorsal part,[33] receives inputs from frontotemporal regions such as inferior frontal gyrus (IFG), dorsolateral PFC (DLPFC), ACC, amygdala, limbic areas, and frontopolar regions. The ventral anterior insula (vAI), also known as the anterior inferior cortex, encompassing the apex, the limen and the transverse gyrus,[34,35] is involved in emotion and empathy processing.[13,21,26,36] The dorsal anterior plays a key role in core cognitive functions including executive control[22,37] decision making, attention, salience processing through its connection with the ACC,[38] task switching, and error and deviancy detection.[1,2,15,17,19,23,24,39–41] Neuroimaging studies have also reported

[1]Helen Wills Neuroscience Institute, University of California, Berkeley, Berkeley, CA, USA
[2]Université de Franche-Comté, SUPMICROTECH, CNRS, Institut FEMTO-ST, 25000 Besançon, France
[3]Université Paris Cité, Institute of Psychiatry and Neuroscience of Paris (IPNP), INSERM U1266, Team TURC, 75014 Paris, France
[4]Department of Neurosurgery, Oslo University Hospital, Oslo, Norway
[5]Department of Neurology and Center for Mind and Brain, University of California, Davis, Davis, CA, USA
[6]Department of Psychology, University of Oslo, Oslo, Norway
[7]RITMO Center for Interdisciplinary Studies in Rhythm, Time and Motion, University of Oslo, Oslo, Norway
[8]Department of Neuropsychology, Helgeland Hospital, Mosjøen, Norway
[9]Department of Psychology, University of California, Berkeley, Berkeley, CA, USA
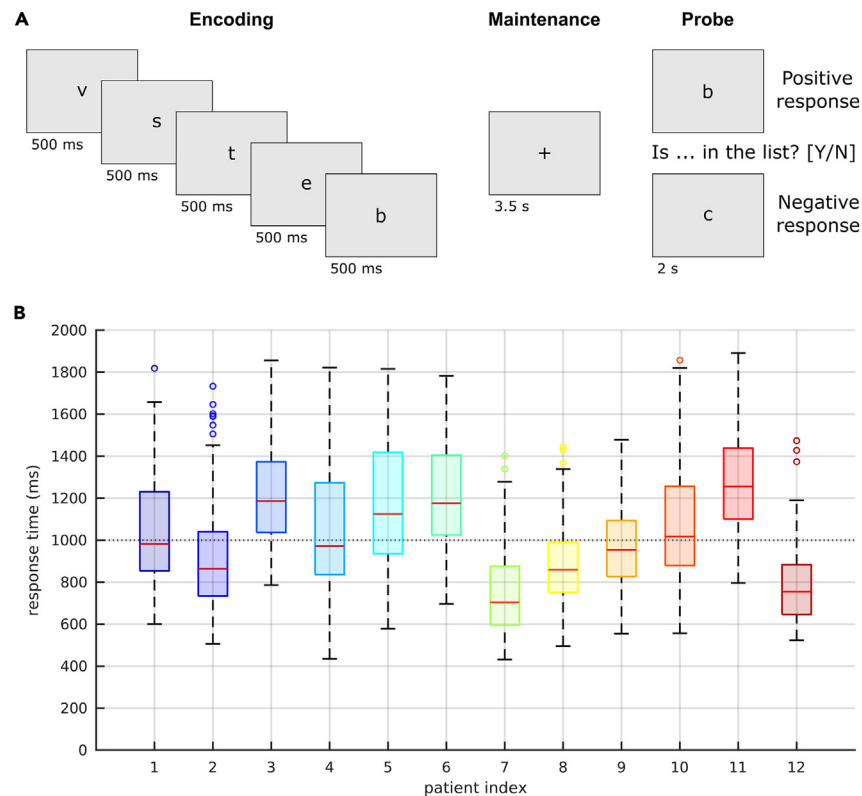[10]These authors contributed equally
[11]Senior authors
[12]Lead contact
*Correspondence: anaisllorens@hotmail.com
https://doi.org/10.1016/j.isci.2023.107653

Figure 1. Task design and behavioral results

(A) Design of the vWM task, composed of 3 phases: encoding of 5 letters, maintenance, and probe. Duration of each screen is displayed below the example frames. During the probe, the correct responses was positive ("yes, the letter was in the list") or negative ("no, it was not in the list").

(B) Response time (RT) distribution of correct trials per participant. For each patient, the red central mark represents the median RT, the bottom and top edges of the box are the 25th and 75th percentiles, respectively, and the lower and upper whiskers are the most extreme non-outlier RTs, respectively.

anterior insula involvement in working memory (WM,[42,43]see[13] for a review) and verbal WM (vWM) processes such as maintenance, interference resolution, and recency effects.[44–51]

This insular posterior to anterior gradient described previously has not been directly tested using a task involving the integration of distinct processes recruiting different subregions of the insula. We hypothesized that high-order processes such as WM, which require a decision and a potential motor response, might engage both anterior and posterior insulae, yet the spatiotemporal dynamics of the insula during WM has not been explored.

Here, we investigated the involvement of the insula during vWM using intracranial electrophysiology (iEEG). We analyzed the spatiotemporal dynamics of different frequency band modulations recorded from electrodes implanted in different subregions of the insula of patients undergoing pre-surgical invasive monitoring for potential treatment of drug-resistant epilepsy.[52] By analyzing different frequency bands, we aimed to provide an extended overview of the anatomo-functional dynamics at play in the insula during the entire vWM process. We focused on theta and beta oscillations as they have been reported as the most prominent spontaneous oscillations in the insula and are preferentially organized along the anterior-posterior axis of the insula.[53] In addition, theta band has been widely reported as the frequency band underpinning important aspects of the (v)WM process.[54,55] We hypothesized that the different phases of vWM will modulate insular theta activity. The specific role of beta bands during WM processes is under debate.[54] We included it in our study to assess its potential involvement in insular function. Lastly, iEEG recordings provide direct access to high frequency activity (HFA), known to be an index of local neuronal population activity.[56–59] HFA has been observed in multiple cognitive processes including WM.[60–62] Based on the extended literature we predicted HFA modulations in the insula related to the decision-making-based probe period. In accordance with this proposal, we assessed the relationship between insular HFA and behavioral performance.

RESULTS

Behavioral results

Twelve patients performed a vWM task requiring them to encode and maintain in memory a list of five successive letters, then to answer whether a probe letter had been presented in the list (Figure 1A). They executed the task well with an average of 79.2% of correct answers
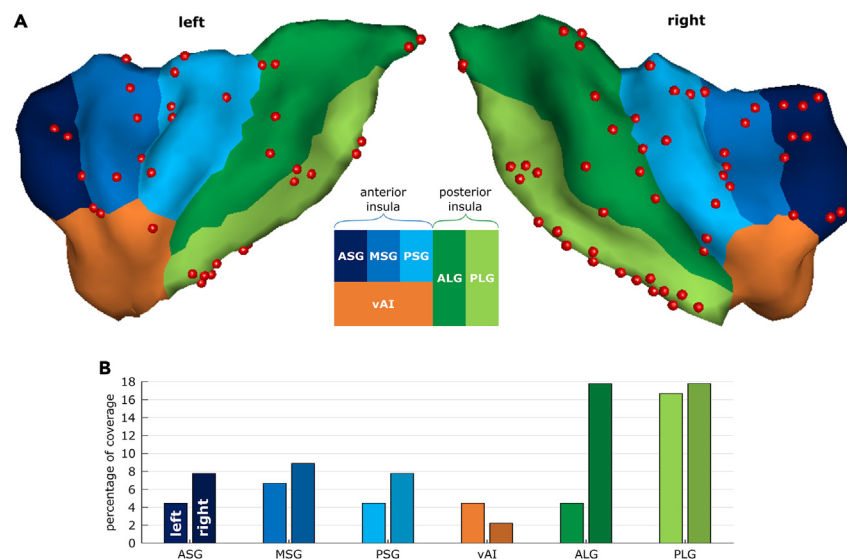
Figure 2. Electrode coverage for each subregion of both insulae

(A) Projection of the 90 electrodes onto the 3D insula reconstructed from the MNI template brain. The color code for the 6 subregions is illustrated by the schematic representation of the different subregions.

(B) Percentage of electrodes in the different subregions of the left (lighter colors) and right (darker colors) insula based on patient-wise localizations. ASG: anterior short gyrus; MSG: middle short gyrus; PSG: posterior short gyrus; vAI: ventral anterior insula; ALG: anterior long gyrus; PLG: posterior long gyrus.

(range 56%–95.1%). The mean response time (RT) across patients was 1031.8 ms (SD 173.6 ms; Figure 1B). No significant correlation was found between RT and accuracy across patients (r = −0.38, p = 0.24). The age of participants was not correlated with RT (p = 0.75) nor with the percentage of correct answers (p = 0.70). No gender effect was found on RT (p = 0.55) or percentage of correct answers (p = 0.43). Correct trials for positive (i.e., probe letter presented in the current list) and negative (i.e., probe letter not presented in the current list) response conditions did not significantly differ in number (total number of correct trials across patients: 654 vs. 694) nor in RT (mean RT of positive vs. negative responses trials across patients: 1036 ms vs. 1030.7 ms).

Electrode coverage in bilateral insulae

Figure 2 shows the overall coverage of the insula. The 90 bipolar channels were distributed over the anterior and posterior regions of both insulae (35 left, 55 right; Figure 2A). In both hemispheres, the posterior long gyrus (PLG) had the largest coverage (16.7% of electrodes in the left insula and 17.8% in the right insula; Figure 2B). The main difference of coverage observed between hemispheres was the proportion of electrodes implanted in the anterior long gyrus (ALG; 4.4% for left vs. 17.8% for right).

Prominent frequency band modulations occurred at the probe period

The linear mixed-effects model comparing frequency activity across the anatomical location of the 90 channels, the three time periods and the three frequency bands, revealed main effects of frequency bands (f(2,803) = 32.4, p < 0.0001) and time periods (f(2,803) = 3.2, p < 0.05) and a trend for laterality (f(1,803) = 2.9, p = 0.09). Post-hoc tests revealed significant effects across the three frequency bands (p < 0.0001 for each of the three tests: theta versus beta, theta versus HFA, and beta versus HFA).

A limited number of channels showed significant time-overlapping modulations (p < 0.05 for at least 25 ms consecutively) during the encoding and maintenance periods of the correct trials for the three neural frequency bands of interest. All the significant modulations (power changes relative to baseline) were found in the right insula (see Figure S1). Significant theta modulations were observed for the encoding (N = 2/12; i.e., 2 channels with significant time-overlapping modulations out of 12 responsive channels in the theta band) and the maintenance (N = 3/15) periods. Beta modulations were found at the end of the encoding (N = 2/8) and some HFA modulations were found at the encoding and the maintenance (N = 3/24 for both time periods). In contrast, prominent insular activity in all three frequency bands was observed at the probe period (p < 0.05). Based on these observations, we focused the rest of the analyses on this probe time window. Among the 90 insular channels, twenty-one were found responsive in theta (23%), 19 in beta (21%), and 39 in HFA (43%). Dynamics patterns of activity were observed across channels for each frequency band of interest (see Figure S2).

In the theta band, 6 out of the 10 responsive channels in the left insula and 7 out of the 11 channels in the right insula showed overlapping significant theta modulation during the probe period. A theta increase was observed 400 ms after the probe presentation in the anterior parts of both insulae (N = 2 out of the 5 channels located in the left anterior insula and N = 2/4 in the right anterior insula) as well as in the right posterior insula (N = 5/7). In the left insula, the theta increase was followed by a theta decrease around 1,400 ms which was larger in its
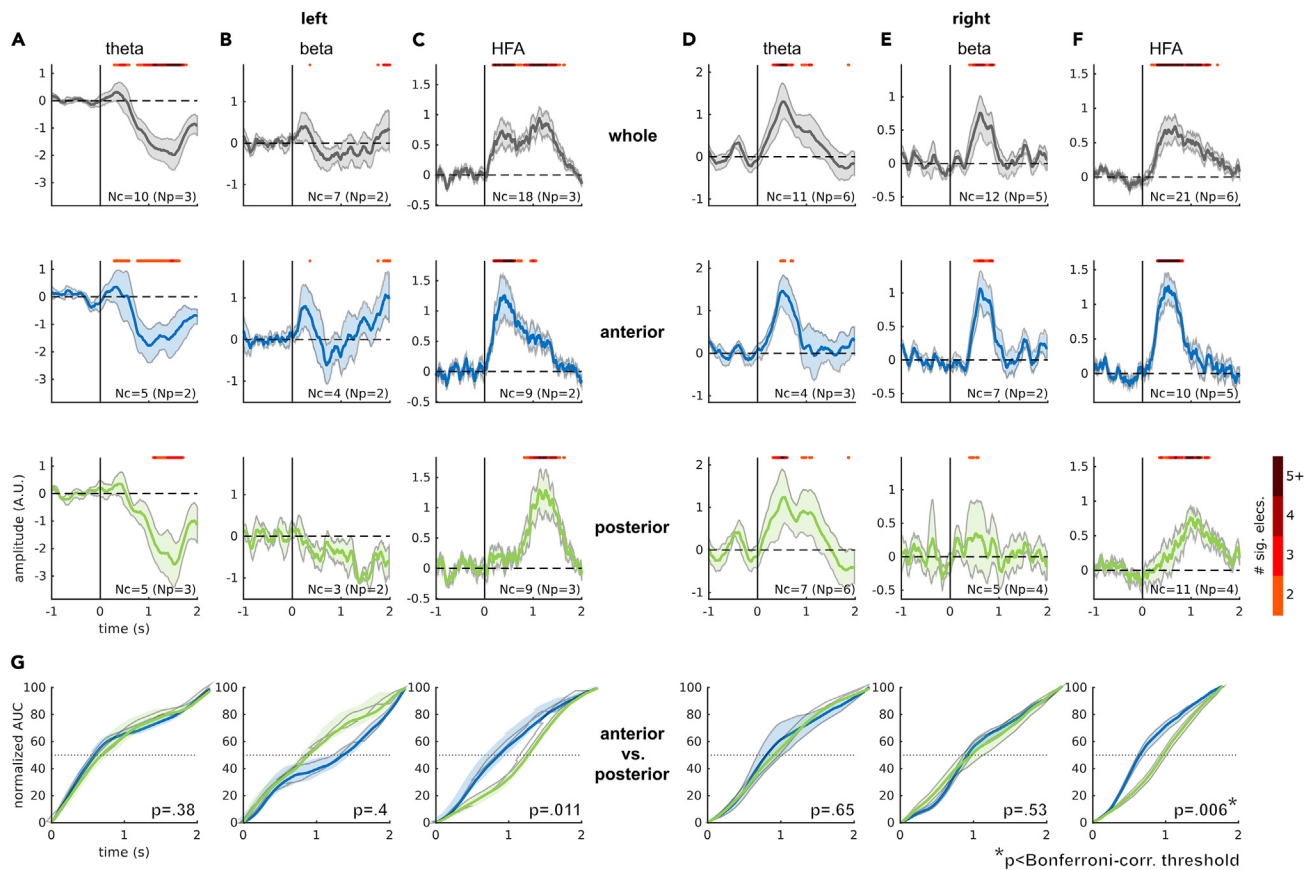
Figure 3. Frequency band modulations at the probe period

(A–F) Time courses of theta, beta, and HFA modulations in the left (A–C) and right (D–F) insulae. Frequency band modulations averaged across all responsive channels (Nc = number of channels; Np = number of participants) for the whole insula (gray), the anterior part (blue), and the posterior part (green). Shaded areas represent the standard error of the mean (SEM). The upper red bar highlights the time points at which at least two channels showed significant modulation. The color code indicates the number of significant channels (the darker the more channels), see also Figure S2 for the time course of each responsive channel at the probe period.

(G) Comparison of the cumulative area under the curve (AUC) for each frequency band modulations between the anterior and posterior parts (blue and green, respectively) of both insulae. The dotted line represents 50% of the normalized AUC. The Bonferroni-corrected alpha threshold is p = 0.008.

posterior part (N = 3/5 left anterior and 3/5 left posterior; see Figures 3A and S2, left panel) while a second peak of theta at 1 s was observed for 2 channels in the right posterior insula (Figure 3D). The latency difference of theta modulations between the anterior and posterior parts of both insulae was not significant (p = 0.38 for the left insula and p = 0.65 for the right insula, Figure 3G).

Overlapping beta band modulations were observed in 2 out of the 7 responsive channels in the left and 4 out of the 12 channels in the right insula. In the left insula, 2 channels showed a beta increase at 2 s after the probe onset (Figures 3B and S2 middle panel). A significant beta increase was found around 650 ms after the probe onset in the right insula, predominantly in its anterior part (N = 3/7 for right anterior insula and N = 2/5 for posterior; Figure 3E). No timing difference was observed in the beta band along the anteroposterior axis of both insulae (left insula: p = 0.4; right insula: p = 0.5).

Finally, overlapping significant HFA modulations were observed in both insulae for 6 out of 18 responsive channels were simultaneously modulated in the left and 12 out of 21 channels in the right insula. An initial increase around 400 ms after the probe onset occurred in the anterior parts of the insulae bilaterally (N = 5/9 for the left anterior insula and 8/10 for the right anterior insula) and a second HFA increase was seen 1s after the probe onset in the posterior insulae bilaterally (N = 5/9 for the left posterior insula and 6/11 for the right posterior insula Figures 3C, 3F, and S2, right panel), with the stronger increase in the left posterior one. The latency analysis confirmed the timing difference for HFA modulations between the anterior and the posterior parts of the right insula (p = 0.006) while a tendency was found for the left insula (p = 0.011, Bonferroni-corrected alpha = 0.05/6 = 0.008, Figure 3G).

Distinct profiles of frequency activity at the probe period

We performed a clustering analysis in order to disentangle the different profiles of frequency modulations observed in the insula. For each of the three frequency bands, we sorted the correct trials by increasing RT and formed 10 sub-averages. The optimal number of clusters of these
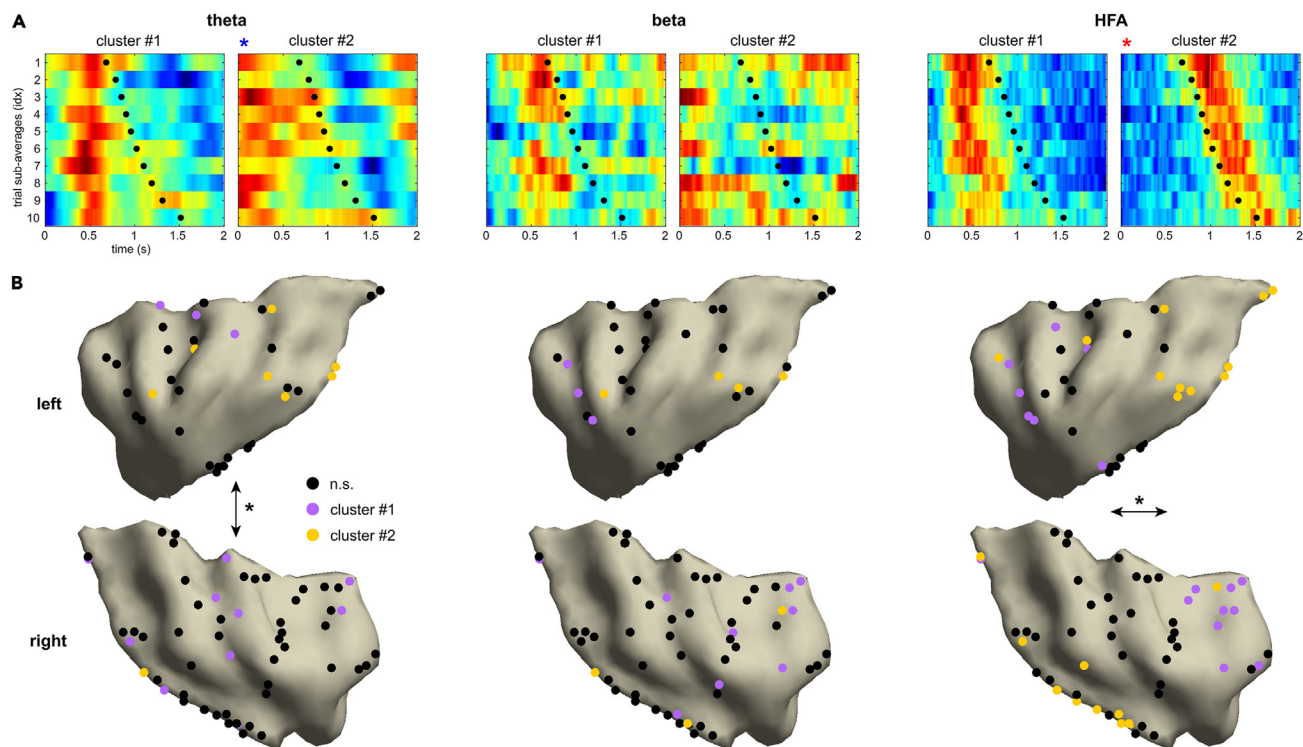
Figure 4. Clustering analysis at the probe period for each of the frequency bands

(A) Cluster centroids as frequency band modulations sorted by increasing RT and sub-averaged, for each frequency band. Black dots represent mean RT across patients. Red represents an increase of frequency power and blue a decrease. Asterisks represent significant correlations between mean RT and peaks (red symbol) or troughs (blue symbol) of frequency band modulations.

(B) Clusters' spatial distribution per frequency band projected onto the 3D MNI insula template, the color of the dots codes for electrode belonging to cluster 1 (purple) or cluster 2 (orange).

sub-averaged time courses estimated over all responsive channels was two and differed in their pattern of frequency modulations (Figure 4A) and anatomical location (Figure 4B).

Theta

The first cluster was composed of 13 channels and showed a theta increase locked at 500 ms after the probe onset, which was not correlated with RT ($r = -0.32$; $p = 0.35$). This pattern of activity was predominantly found in the right insula with 10 channels (2 ASG, 1 MSG, 1 PSG, 3 ALG, and 3 PLG) compared to 3 channels in the left insula (2 MSG and 1 ALG; Figure 4, left column). The second cluster revealed a theta increase at the probe onset, followed by a theta decrease with its trough correlated with RT ($r = -0.88$; $p < 0.001$). The 8 channels showing this pattern were all located in the left insula (1 MSG, 1 PSG, 1 vAI, 1 ALG, and 3 PLG), except for one (right PLG). The 7 channels in the left insula were ipsilateral to the response hand used by 2 participants of this cluster while the electrode in the right insula was contralateral to the hand used by the third participant. The spatial distribution of channels across these two clusters was significantly different between the right and left insulae (Fisher's exact test, $p < 0.01$) but not along the anteroposterior axis ($p = 1$).

Beta

The first cluster encompassed 12 channels, predominantly in the right hemisphere (right: 3 ASG, 2 MSG, 1 vAI, 2 ALG, and 1 PLG; left: 2 ASG and 1 ALG), and showed a beta increase 500 ms after the probe onset. The second cluster showed a beta increase at the probe onset in 7 channels located in both insulae, with 3 channels in the anterior insula and 4 in the posterior insula (right: 1 vAI, 1 ALG, and 2 PLG; left: 1 MSG and 2 PLG). None of these clusters correlated significantly with RT ($r = -0.68$; $p = 0.03$ and $r = 0.42$; $p = 0.23$ for cluster 1 and 2 respectively; Figure 4, middle column). The spatial distribution of channels across clusters was not statistically different between hemispheres ($p = 0.33$) nor along the anteroposterior axis ($p = 0.074$).

HFA

The first HFA cluster encompassed 17 channels showing an HFA increase 500 ms after the probe onset, not correlated with RT ($r = 0.39$; $p = 0.26$). These channels were located predominantly in the anterior parts of both insulae (anterior insula: 8; ASG: 4 right/3 left, 7

MSG: 5 right/2left, 1 left vAI; posterior insula: 1 right ALG, and 1 left PLG). The second cluster was composed of 22 channels with an increase of HFA occurring after the button press. The peak of HFA was correlated with RT (r = −0.95; p < 0.001; Figure 4, right column). This modulation was predominantly observed in the posterior parts of both insulae (18 channels in posterior insula: 5 ALG: 2 right/3 left and 13 PLG: 8 right/5 left; 4 channels in anterior insula: 1 right ASG, 2 right PSG, and 1 left ASG). These 22 channels were all located in the insula ipsilateral to the hand used by the 7 participants for whom channels were included in this cluster. The spatial distribution of channels across the HFA clusters was significantly different along the anteroposterior axis (p < 0.0001) but not between insulae (p = 0.75).

DISCUSSION

Our study provides intracranial electrophysiological evidence for distributed spatiotemporal involvement of the human insula in the decision-making process required during the probe period of a vWM task. We investigated the power modulations elicited by vWM processes in three neural frequency bands within the insula. We demonstrated that the task elicited a variety of different frequency band modulations. First, we observed that the encoding and the maintenance periods elicit only a few frequency band modulations for transient periods of time mainly in the right insula. Theta oscillations are known to be critically involved in (v)WM processes.[54,55] However, they are marginally observed during the encoding and the maintenance in our study. These results indicate that the insula might not be strongly recruited during these two time periods.

We found that the probe period elicited the strongest insula involvement, with interhemispheric and sequential intra-insular asymmetries observed across all frequency bands. The probe period elicited differential involvement of the left and right insula in theta band and, to some extent in the beta band, as well as along their anteroposterior axes in HFA.

The interhemispheric asymmetry observed in the theta band may be due to differential roles, with the right insula being potentially more involved in the attentional aspect of the task[1,21,22] and the left insula in the linguistic aspect.[43,47] Interestingly, a theta decrease was correlated with RT in the left insula. Theta decrease during WM has also been observed in a few electrophysiology studies using scalp EEG (see[54,63] for reviews) and iEEG.[64] Another iEEG study showed that a theta decrease in the DLPFC was predictive of WM performance.[65] Moreover, multiple iEEG studies have reported a theta decrease, or reset, especially in the left MTL, related to successful memory retrieval.[66–71] In our study, it is interesting to note that 5 out of the 7 channels in the left insula showing a decrease of theta after the RT also showed an increase of HFA during the same time period. These results are in line with literature reporting a decrease of theta power and increase of HFA power in fronto-temporal regions during successful retrieval[66,72] as well as successful memory encoding.[67]

Limited spatial clustering and functional activity observed in the beta band prevented us from drawing strong conclusions about its potential role in vWM processes. These results are in agreement with the recent review by Pavlov and Kotchoubey 2022,[54] where the authors discuss the lack of agreement regarding the beta modulations during WM reported in the EEG and MEG literature. Another potential explanation could come from the fact that beta oscillations have been reported mostly in the anterior part of the insula.[53] Our lack of coverage in the most anterior ventral part of the insula precludes us from making strong claims about the absence of clear beta modulations and clustering.

The time course of HFA revealed sequential activity in the insulae along an anteroposterior axis. Interestingly, limited anatomical overlapping was observed across the two HFA clusters, in line with functional differentiation between the anterior and posterior insula.[21,27] The anterior insulae were active at the probe presentation while subsequent posterior activity occurred after the behavioral response. The early HFA modulation in anterior insula provides evidence of its involvement in decision making related to the encoded verbal material,[47,51] supporting the assertion that the AIC is a crucial part of the cognitive control network.[37,40,73–75] The posterior insula has been reported to be involved in motor activity due to its connection with the SMA.[1,2] However, the HFA increase that correlated with RT in our study occurred after the motor response and was only found in the insula ipsilateral to the motor activity. This observation does not support a role of the posterior insula in pure motor preparation or activation.[24,29,76] Instead, our findings support a key role in response monitoring, potentially achieved through its connection with the cingulate gyrus[7,77] and the sensory-motor system.[24,33,36,78] The posterior insula may monitor the sensorimotor information triggered by the motor response[78–81] and integrate it with the cognitive information originating from the anterior part of the insula. Further studies will be needed to better characterize the role of the posterior insula in monitoring behavior. In sum, our present study implicates the insula throughout the vWM process, with a critical sequential involvement during the decision making and response monitoring phases.

Limitations of the study

Our study has the well-known limitations inherent to studies of intracerebral activity in epileptic patients.[61,62] This population may show inter-individual variability at different levels. First, there is heterogeneity of epileptic networks and potential functional reorganizations associated with it. To address this, we removed any abnormal data and channels from our analyses, resulting in the exclusion of two patients and individual electrodes in some of the remaining twelve subjects. We note that multiple prior iEEG studies adopting this strategy have reported iEEG activity in accord with findings from fMRI and lesion analysis in a vast number of cognitive processes.[60,61,82–84] Second, there is a heterogeneity of cognitive abilities across patients (e.g., poor memory abilities which could interfere with performance). In order to minimize this effect, we only included in our study patients who performed the task with a performance well above chance level and had an IQ score above 80.

In order to confirm the role of the posterior insula in response monitoring, we ran the same analysis pipeline over incorrect trials and no-response trials. Unfortunately, we did not find enough significant channels in any frequency band to perform a robust analysis.

Finally, we acknowledge the relatively low number of insular electrodes which is a common limitation in the iEEG literature.[28,62,85] The lack of coverage in the most ventral anterior part of the insula, did not allow us to make any claims on the role of this subregion during the vWM

process. In the same vein, some electrodes included here could have been implanted in subinsular areas. To prevent this, we verified the anatomical location of each electrode included in this study based on the individual subject's anatomy and we used a bipolar montage which limits the neural activity recorded to less than 5 mm around the virtual bipolar channel.[61]

STAR★METHODS

Detailed methods are provided in the online version of this paper and include the following:

- KEY RESOURCES TABLE
- RESOURCE AVAILABILITY
  - Lead contact
  - Materials availability
  - Data and code availability
- EXPERIMENTAL MODEL AND STUDY PARTICIPANT DETAILS
  - Human participants
- METHOD DETAILS
  - Electrode localization
  - 3D insula model reconstruction
  - Experimental task and setup
  - Behavioral analysis
  - SEEG data acquisition and preprocessing
- QUANTIFICATION AND STATISTICAL ANALYSIS
  - Analyses over the entire vWM process
  - Analyses at the probe period
  - Correlation with behavioral response time

SUPPLEMENTAL INFORMATION

Supplemental information can be found online at https://doi.org/10.1016/j.isci.2023.107653.

AUTHOR CONTRIBUTIONS

Conceptualization: T.E., A.-K.S., A.L., and L.B. Methodology and Analysis: L.B. and A.L. Investigation: A.L., L.B., and A.O.B. Resources: J.I., P.G.L., and J.J.L. Writing – Original: A.L., L.B., and R.T.K. Writing – Review and Editing: A.O.B., J.I., P.G.L., J.J.L., T.E., and A.-K.S. Supervision and funding acquisition: T.E., A.-K.S., and R.T.K.

DECLARATION OF INTERESTS

The authors declare no competing interests.

INCLUSION AND DIVERSITY

While citing references scientifically relevant for this work, we also actively worked to promote gender balance in our reference list.[86–88]

REFERENCES

1. Menon, V., and Uddin, L.Q. (2010). Saliency, switching, attention and control: a network model of insula function. Brain Struct. Funct. *214*, 655–667. https://doi.org/10.1007/s00429-010-0262-0.

2. Uddin, L.Q., Nomi, J.S., Hébert-Seropian, B., Ghaziri, J., and Boucher, O. (2017). Structure and function of the human insula. J. Clin. Neurophysiol. *34*, 300–306. https://doi.org/10.1097/WNP.0000000000000377.

3. Reil, J.C. (1809). Die sylvische Grube. Archiv für die Physiologie 9, 195–208.

4. Flynn, F.G. (1999). Anatomy of the insula functional and clinical correlates. Aphasiology *13*, 55–78. https://doi.org/10.1080/026870399402325.

5. Namkung, H., Kim, S.-H., and Sawa, A. (2017). The Insula: An Underestimated Brain Area in Clinical Neuroscience, Psychiatry, and Neurology. Trends Neurosci. *40*, 200–207. https://doi.org/10.1016/j.tins.2017.02.002.

6. Gasquoine, P.G. (2014). Contributions of the Insula to Cognition and Emotion. Neuropsychol. Rev. *24*, 77–87. https://doi.org/10.1007/s11065-014-9246-9.

7. Ghaziri, J., Tucholka, A., Girard, G., Houde, J.-C., Boucher, O., Gilbert, G., Descoteaux, M., Lippé, S., Rainville, P., and Nguyen, D.K. (2017). The Corticocortical Structural Connectivity of the Human Insula. Cereb. Cortex *27*, 1216–1228. https://doi.org/10.1093/cercor/bhv308.

8. Cacciola, A., Calamuneri, A., Milardi, D., Mormina, E., Chillemi, G., Marino, S., Naro, A., Rizzo, G., Anastasi, G., and Quartarone, A. (2017). A Connectomic Analysis of the Human Basal Ganglia Network. Front. Neuroanat. 11, 85.

9. Fudge, J.L., Breitbart, M.A., Danish, M., and Pannoni, V. (2005). Insular and gustatory inputs to the caudal ventral striatum in primates. J. Comp. Neurol. *490*, 101–118. https://doi.org/10.1002/cne.20660.

10. Augustine, J.R. (1996). Circuitry and functional aspects of the insular lobe in primates including humans. Brain Res. Brain Res. Rev. *22*, 229–244. https://doi.org/10.1016/s0165-0173(96)00011-2.

11. Mesulam, M.M., and Mufson, E.J. (1982). Insula of the old world monkey. III: Efferent cortical output and comments on function. J. Comp. Neurol. *212*, 38–52. https://doi.org/10.1002/cne.902120104.

12. Shelley, B.P., and Trimble, M.R. (2004). The insular Lobe of Reil—its Anatamico-Functional, behavioural and Neuropsychiatric attributes in humans—a review. World J. Biol. Psychiatry *5*, 176–200. https://doi.org/10.1080/15622970410029933.

13. Kurth, F., Zilles, K., Fox, P.T., Laird, A.R., and Eickhoff, S.B. (2010). A link between the systems: functional differentiation and integration within the human insula revealed by meta-analysis. Brain Struct. Funct. *214*, 519–534. https://doi.org/10.1007/s00429-010-0255-z.

14. Wang, Y., Zou, Q., Ao, Y., Liu, Y., Ouyang, Y., Wang, X., Biswal, B., Cui, Q., and Chen, H. (2020). Frequency-dependent circuits anchored in the dorsal and ventral left anterior insula. Sci. Rep. *10*, 16394. https://doi.org/10.1038/s41598-020-73192-z.

15. Wang, Y., Zhu, L., Zou, Q., Cui, Q., Liao, W., Duan, X., Biswal, B., and Chen, H. (2018). Frequency dependent hub role of the dorsal and ventral right anterior insula. Neuroimage *165*, 112–117. https://doi.org/10.1016/j.neuroimage.2017.10.004.

16. Cosentino, S., Brickman, A.M., Griffith, E., Habeck, C., Cines, S., Farrell, M., Shaked, D., Huey, E.D., Briner, T., and Stern, Y. (2015). The right insula contributes to memory awareness in cognitively diverse older adults. Neuropsychologia *75*, 163–169. https://doi.org/10.1016/j.neuropsychologia.2015.05.032.

17. Craig, A.D.B. (2009). How do you feel–now? The anterior insula and human awareness. Nat. Rev. Neurosci. *10*, 59–70. https://doi.org/10.1038/nrn2555.

18. Oh, A., Duerden, E.G., and Pang, E.W. (2014). The role of the insula in speech and language processing. Brain Lang. *135*, 96–103. https://doi.org/10.1016/j.bandl.2014.06.003.

19. Ullsperger, M., Harsay, H.A., Wessel, J.R., and Ridderinkhof, K.R. (2010). Conscious perception of errors and its relation to the anterior insula. Brain Struct. Funct. *214*, 629–643. https://doi.org/10.1007/s00429-010-0261-1.

20. Wager, T.D., Jonides, J., and Reading, S. (2004). Neuroimaging studies of shifting attention: a meta-analysis. Neuroimage *22*, 1679–1693. https://doi.org/10.1016/j.neuroimage.2004.03.052.

21. Uddin, L.Q., Kinnison, J., Pessoa, L., and Anderson, M.L. (2014). Beyond the tripartite cognition-emotion-interoception model of the human insular cortex. J. Cogn. Neurosci. *26*, 16–27. https://doi.org/10.1162/jocn_a_00462.

22. Cauda, F., Costa, T., Torta, D.M.E., Sacco, K., D'Agata, F., Duca, S., Geminiani, G., Fox, P.T., and Vercelli, A. (2012). Meta-analytic clustering of the insular cortex Characterizing the meta-analytic connectivity of the insula when involved in active tasks. Neuroimage *62*, 343–355. https://doi.org/10.1016/j.neuroimage.2012.04.012.

23. Citherlet, D., Boucher, O., Tremblay, J., Robert, M., Gallagher, A., Bouthillier, A., Lepore, F., and Nguyen, D.K. (2020). Spatiotemporal dynamics of auditory information processing in the insular cortex: an intracranial EEG study using an oddball paradigm. Brain Struct. Funct. *225*, 1537–1559. https://doi.org/10.1007/s00429-020-02072-z.

24. Citherlet, D., Boucher, O., Tremblay, J., Robert, M., Gallagher, A., Bouthillier, A., Lepore, F., and Nguyen, D.K. (2019). Role of the insula in top–down processing: an intracranial EEG study using a visual oddball detection paradigm. Brain Struct. Funct. *224*, 2045–2059. https://doi.org/10.1007/s00429-019-01892-y.

25. Tian, Y., and Zalesky, A. (2018). Characterizing the functional connectivity diversity of the insula cortex: Subregions, diversity curves and behavior. Neuroimage *183*, 716–733. https://doi.org/10.1016/j.neuroimage.2018.08.055.

26. Kelly, C., Toro, R., Di Martino, A., Cox, C.L., Bellec, P., Castellanos, F.X., and Milham, M.P. (2012). A convergent functional architecture of the insula emerges across imaging modalities. Neuroimage *61*, 1129–1142. https://doi.org/10.1016/j.neuroimage.2012.03.021.

27. Nomi, J.S., Farrant, K., Damaraju, E., Rachakonda, S., Calhoun, V.D., and Uddin, L.Q. (2016). Dynamic functional network connectivity reveals unique and overlapping profiles of insula subdivisions. Hum. Brain Mapp. *37*, 1770–1787. https://doi.org/10.1002/hbm.23135.

28. Blenkmann, A.O., Collavini, S., Lubell, J., Llorens, A., Funderud, I., Ivanovic, J., Larsson, P.G., Meling, T.R., Bekinschtein, T., Kochen, S., et al. (2019). Auditory deviance detection in the human insula: An intracranial EEG study. Cortex *121*, 189–200. https://doi.org/10.1016/j.cortex.2019.09.002.

29. Taylor, K.S., Seminowicz, D.A., and Davis, K.D. (2009). Two systems of resting state connectivity between the insula and cingulate cortex. Hum. Brain Mapp. *30*, 2731–2745. https://doi.org/10.1002/hbm.20705.

30. Woolnough, O., Forseth, K.J., Rollo, P.S., and Tandon, N. (2019). Uncovering the functional anatomy of the human insula during speech. Elife *8*, e53086. https://doi.org/10.7554/eLife.53086.

31. Zhang, Y., Zhou, W., Wang, S., Zhou, Q., Wang, H., Zhang, B., Huang, J., Hong, B., and Wang, X. (2019). The Roles of Subdivisions of Human Insula in Emotion Perception and Auditory Processing. Cereb. Cortex *29*, 517–528. https://doi.org/10.1093/cercor/bhx334.

32. Hsueh, B., Chen, R., Jo, Y., Tang, D., Raffiee, M., Kim, Y.S., Inoue, M., Randles, S., Ramakrishnan, C., Patel, S., et al. (2023). Cardiogenic control of affective behavioural state. Nature *615*, 292–299. https://doi.org/10.1038/s41586-023-05748-8.

33. Deen, B., Pitskel, N.B., and Pelphrey, K.A. (2011). Three Systems of Insular Functional Connectivity Identified with Cluster Analysis. Cereb. Cortex *21*, 1498–1506. https://doi.org/10.1093/cercor/bhq186.

34. Faillenot, I., Heckemann, R.A., Frot, M., and Hammers, A. (2017). Macroanatomy and 3D probabilistic atlas of the human insula. Neuroimage *150*, 88–98. https://doi.org/10.1016/j.neuroimage.2017.01.073.

35. Fathy, Y.Y., Hepp, D.H., de Jong, F.J., Geurts, J.J.G., Foncke, E.M.J., Berendse, H.W., van de Berg, W.D.J., and Schoonheim, M.M. (2020). Anterior insular network disconnection and cognitive impairment in Parkinson's disease. Neuroimage. Clin. *28*, 102364. https://doi.org/10.1016/j.nicl.2020.102364.

36. Chang, L.J., Yarkoni, T., Khaw, M.W., and Sanfey, A.G. (2013). Decoding the Role of the Insula in Human Cognition: Functional Parcellation and Large-Scale Reverse Inference. Cereb. Cortex *23*, 739–749. https://doi.org/10.1093/cercor/bhs065.

37. Molnar-Szakacs, I., and Uddin, L.Q. (2022). Anterior insula as a gatekeeper of executive control. Neurosci. Biobehav. Rev. *139*, 104736. https://doi.org/10.1016/j.neubiorev.2022.104736.

38. Das, A., and Menon, V. (2020). Spatiotemporal Integrity and Spontaneous Nonlinear Dynamic Properties of the Salience Network Revealed by Human Intracranial Electrophysiology: A Multicohort Replication. Cereb. Cortex *30*, 5309–5321. https://doi.org/10.1093/cercor/bhaa111.

39. Cole, M.W., and Schneider, W. (2007). The cognitive control network: Integrated cortical regions with dissociable functions. Neuroimage *37*, 343–360. https://doi.org/10.1016/j.neuroimage.2007.03.071.

40. Droutman, V., Bechara, A., and Read, S.J. (2015). Roles of the Different Sub-Regions of the Insular Cortex in Various Phases of the Decision-Making Process. Front. Behav. Neurosci. 9, 309.

41. Wager, T.D., and Barrett, L.F. (2017). From affect to control: Functional specialization of the insula in motivation and regulation. Preprint at BiorXiv102368. https://doi.org/10.1101/102368.

42. Chang, C., Crottaz-Herbette, S., and Menon, V. (2007). Temporal dynamics of basal ganglia response and connectivity during verbal working memory. Neuroimage *34*, 1253–1269. https://doi.org/10.1016/j.neuroimage.2006.08.056.

43. Wager, T.D., and Smith, E.E. (2003). Neuroimaging studies of working memory: Cognitive, Affective. Cogn. Affect. Behav. Neurosci. *3*, 255–274. https://doi.org/10.3758/CABN.3.4.255.

44. D'Esposito, M., Postle, B.R., Ballard, D., and Lease, J. (1999). Maintenance versus Manipulation of Information Held in Working Memory: An Event-Related fMRI Study. Brain Cogn. *41*, 66–86. https://doi.org/10.1006/brcg.1999.1096.

45. Jonides, J., Smith, E.E., Marshuetz, C., Koeppe, R.A., and Reuter-Lorenz, P.A. (1998). Inhibition in verbal working memory revealed by brain activation. Proc. Natl. Acad. Sci. USA 95, 8410–8413.

46. Levens, S.M., and Phelps, E.A. (2010). Insula and Orbital Frontal Cortex Activity Underlying Emotion Interference Resolution in Working Memory. J. Cogn. Neurosci. *22*, 2790–2803. https://doi.org/10.1162/jocn.2010.21428.

47. Marvel, C.L., and Desmond, J.E. (2012). From storage to manipulation: How the neural correlates of verbal working memory reflect varying demands on inner speech. Brain Lang. *120*, 42–51. https://doi.org/10.1016/j.bandl.2011.08.005.

48. Marvel, C.L., and Desmond, J.E. (2010). The contributions of cerebro-cerebellar circuitry to executive verbal working memory. Cortex *46*, 880–895. https://doi.org/10.1016/j.cortex.2009.08.017.

49. Nee, D.E., Jonides, J., and Berman, M.G. (2007). Neural mechanisms of proactive interference-resolution. Neuroimage *38*, 740–751. https://doi.org/10.1016/j.neuroimage.2007.07.066.

50. Schulze, K., Zysset, S., Mueller, K., Friederici, A.D., and Koelsch, S. (2011). Neuroarchitecture of verbal and tonal working memory in nonmusicians and musicians. Hum. Brain Mapp. *32*, 771–783. https://doi.org/10.1002/hbm.21060.

51. Wager, T.D., Sylvester, C.-Y.C., Lacey, S.C., Nee, D.E., Franklin, M., and Jonides, J. (2005). Common and unique components of response inhibition revealed by fMRI. Neuroimage *27*, 323–340. https://doi.org/10.1016/j.neuroimage.2005.01.054.

52. Abou-Al-Shaar, H., Brock, A.A., Kundu, B., Englot, D.J., and Rolston, J.D. (2018). Increased nationwide use of stereoencephalography for intracranial epilepsy electroencephalography recordings. J. Clin. Neurosci. *53*, 132–134. https://doi.org/10.1016/j.jocn.2018.04.064.

53. Das, A., Myers, J., Mathura, R., Shofty, B., Metzger, B.A., Bijanki, K., Wu, C., Jacobs, J., and Sheth, S.A. (2022). Spontaneous neuronal oscillations in the human insula are hierarchically organized traveling waves. Elife *11*, e76702. https://doi.org/10.7554/eLife.76702.

54. Pavlov, Y.G., and Kotchoubey, B. (2022). Oscillatory brain activity and maintenance of verbal and visual working memory: A systematic review. Psychophysiology *59*, e13735. https://doi.org/10.1111/psyp.13735.

55. Roux, F., and Uhlhaas, P.J. (2014). Working memory and neural oscillations: alpha–gamma versus theta–gamma codes for distinct WM information? Trends Cogn. Sci. *18*, 16–25. https://doi.org/10.1016/j.tics.2013.10.010.

56. Leszczyński, M., Barczak, A., Kajikawa, Y., Ulbert, I., Falchier, A.Y., Tal, I., Haegens, S., Melloni, L., Knight, R.T., and Schroeder, C.E. (2020). Dissociation of broadband high-frequency activity and neuronal firing in the neocortex. Sci. Adv. *6*, eabb0977. https://doi.org/10.1126/sciadv.abb0977.

57. Nir, Y., Fisch, L., Mukamel, R., Gelbard-Sagiv, H., Arieli, A., Fried, I., and Malach, R. (2007). Coupling between neuronal firing rate, gamma LFP, and BOLD fMRI is related to interneuronal correlations. Curr. Biol. *17*, 1275–1285. https://doi.org/10.1016/j.cub.2007.06.066.

58. Ray, S., Crone, N.E., Niebur, E., Franaszczuk, P.J., and Hsiao, S.S. (2008). Neural Correlates of High-Gamma Oscillations (60–200 Hz) in Macaque Local Field Potentials and Their Potential Implications in Electrocorticography. J. Neurosci. *28*, 11526–11536. https://doi.org/10.1523/JNEUROSCI.2848-08.2008.

59. Rich, E.L., and Wallis, J.D. (2017). Spatiotemporal dynamics of information encoding revealed in orbitofrontal high-gamma. Nat. Commun. *8*, 1139. https://doi.org/10.1038/s41467-017-01253-5.

60. Johnson, E.L., Kam, J.W.Y., Tzovara, A., and Knight, R.T. (2020). Insights into human cognition from intracranial EEG: A review of audition, memory, internal cognition, and causality. J. Neural. Eng. *17*, 051001. https://doi.org/10.1088/1741-2552/abb7a5.

61. Lachaux, J.-P., Axmacher, N., Mormann, F., Halgren, E., and Crone, N.E. (2012). High-frequency neural activity and human cognition: Past, present and possible future of intracranial EEG research. Prog. Neurobiol. *98*, 279–301. https://doi.org/10.1016/j.pneurobio.2012.06.008.

62. Mercier, M.R., Dubarry, A.-S., Tadel, F., Avanzini, P., Axmacher, N., Cellier, D., Vecchio, M.D., Hamilton, L.S., Hermes, D., Kahana, M.J., et al. (2022). Advances in human intracranial electroencephalography research, guidelines and good practices. Neuroimage *260*, 119438. https://doi.org/10.1016/j.neuroimage.2022.119438.

63. Pavlov, Y.G., and Kotchoubey, B. (2020). The electrophysiological underpinnings of variation in verbal working memory capacity. Sci. Rep. *10*, 16900. https://doi.org/10.1038/s41598-020-72940-5.

64. Meltzer, J.A., Zaveri, H.P., Goncharova, I.I., Distasio, M.M., Papademetris, X., Spencer, S.S., Spencer, D.D., and Constable, R.T. (2008). Effects of Working Memory Load on Oscillatory Power in Human Intracranial EEG. Cereb. Cortex *18*, 1843–1855. https://doi.org/10.1093/cercor/bhm213.

65. Brzezicka, A., Kamiński, J., Reed, C.M., Chung, J.M., Mamelak, A.N., and Rutishauser, U. (2019). Working Memory Load-related Theta Power Decreases in Dorsolateral Prefrontal Cortex Predict Individual Differences in Performance. J. Cogn. Neurosci. *31*, 1290–1307. https://doi.org/10.1162/jocn_a_01417.

66. Burke, J.F., Zaghloul, K.A., Jacobs, J., Williams, R.B., Sperling, M.R., Sharan, A.D., and Kahana, M.J. (2013). Synchronous and Asynchronous Theta and Gamma Activity during Episodic Memory Formation. J. Neurosci. *33*, 292–304. https://doi.org/10.1523/JNEUROSCI.2057-12.2013.

67. Greenberg, J.A., Burke, J.F., Haque, R., Kahana, M.J., and Zaghloul, K.A. (2015). Decreases in theta and increases in high frequency activity underlie associative memory encoding. Neuroimage *114*, 257–263. https://doi.org/10.1016/j.neuroimage.2015.03.077.

68. Herweg, N.A., Solomon, E.A., and Kahana, M.J. (2020). Theta Oscillations in Human Memory. Trends Cogn. Sci. *24*, 208–227. https://doi.org/10.1016/j.tics.2019.12.006.

69. Kota, S., Rugg, M.D., and Lega, B.C. (2020). Hippocampal Theta Oscillations Support Successful Associative Memory Formation. J. Neurosci. *40*, 9507–9518. https://doi.org/10.1523/JNEUROSCI.0767-20.2020.

70. Mormann, F., Fell, J., Axmacher, N., Weber, B., Lehnertz, K., Elger, C.E., and Fernández, G. (2005). Phase/amplitude reset and theta–gamma interaction in the human medial temporal lobe during a continuous word recognition memory task. Hippocampus *15*, 890–900. https://doi.org/10.1002/hipo.20117.

71. Tesche, C.D., and Karhu, J. (2000). Theta oscillations index human hippocampal activation during a working memory task. Proc. Natl. Acad. Sci. USA *97*, 919–924. https://doi.org/10.1073/pnas.97.2.919.

72. Burke, J.F. (2014). Spatiotemporal Dynamics of Neural Activity during Human Episodic Memory Encoding and Retrieval (University of Pennsylvania).

73. Dosenbach, N.U.F., Fair, D.A., Miezin, F.M., Cohen, A.L., Wenger, K.K., Dosenbach, R.A.T., Fox, M.D., Snyder, A.Z., Vincent, J.L., Raichle, M.E., et al. (2007). Distinct brain networks for adaptive and stable task control in humans. Proc. Natl. Acad. Sci. USA *104*, 11073–11078. https://doi.org/10.1073/pnas.0704320104.

74. Dosenbach, N.U.F., Visscher, K.M., Palmer, E.D., Miezin, F.M., Wenger, K.K., Kang, H.C., Burgund, E.D., Grimes, A.L., Schlaggar, B.L., and Petersen, S.E. (2006). A core system for the implementation of task sets. Neuron *50*, 799–812. https://doi.org/10.1016/j.neuron.2006.04.031.

75. Wu, T., Wang, X., Wu, Q., Spagna, A., Yang, J., Yuan, C., Wu, Y., Gao, Z., Hof, P.R., and Fan, J. (2019). Anterior insular cortex is a bottleneck of cognitive control. Neuroimage *195*, 490–504. https://doi.org/10.1016/j.neuroimage.2019.02.042.

76. Pessoa, L., Gutierrez, E., Bandettini, P., and Ungerleider, L. (2002). Neural Correlates of Visual Working Memory: fMRI Amplitude Predicts Task Performance. Neuron *35*, 975–987. https://doi.org/10.1016/S0896-6273(02)00817-6.

77. Leech, R., and Smallwood, J. (2019). Chapter 5 - The posterior cingulate cortex: Insights from structure and function. In Handbook of Clinical Neurology Cingulate Cortex, B.A.

Vogt, ed. (Elsevier), pp. 73–85. https://doi.org/10.1016/B978-0-444-64196-0.00005-4.

78. Craig, A.D. (2002). How do you feel? Interoception: the sense of the physiological condition of the body. Nat. Rev. Neurosci. *3*, 655–666. https://doi.org/10.1038/nrn894.

79. Limanowski, J., Lopes, P., Keck, J., Baudisch, P., Friston, K., and Blankenburg, F. (2020). Action-Dependent Processing of Touch in the Human Parietal Operculum and Posterior Insula. Cereb. Cortex *30*, 607–617. https://doi.org/10.1093/cercor/bhz111.

80. Klein, T.A., Ullsperger, M., and Danielmeier, C. (2013). Error awareness and the insula: links to neurological and psychiatric diseases. Front. Hum. Neurosci. *7*, 14.

81. Lovero, K.L., Simmons, A.N., Aron, J.L., and Paulus, M.P. (2009). Anterior insular cortex anticipates impending stimulus significance. Neuroimage *45*, 976–983. https://doi.org/10.1016/j.neuroimage.2008.12.070.

82. Lachaux, J.P., Rudrauf, D., and Kahane, P. (2003). Intracranial EEG and human brain mapping. J. Physiol. Paris *97*, 613–628. https://doi.org/10.1016/j.jphysparis.2004.01.018.

83. Kam, J.W.Y., Mittner, M., and Knight, R.T. (2022). Mind-wandering: mechanistic insights from lesion, tDCS, and iEEG. Trends Cogn. Sci. *26*, 268–282. https://doi.org/10.1016/j.tics.2021.12.005.

84. Hwang, D.Y., and Golby, A.J. (2006). The brain basis for episodic memory: Insights from functional MRI, intracranial EEG, and patients with epilepsy. Epilepsy Behav. *8*, 115–126. https://doi.org/10.1016/j.yebeh.2005.09.009.

85. Saint Amour di Chanaz, L., Pérez-Bellido, A., Wu, X., Lozano-Soldevilla, D., Pacheco-Estefan, D., Lehongre, K., Conde-Blanco, E., Roldan, P., Adam, C., Lambrecq, V., et al. (2023). Gamma amplitude is coupled to opposed hippocampal theta-phase states during the encoding and retrieval of episodic memories in humans. Curr. Biol. *33*, 1836–1843.e6. https://doi.org/10.1016/j.cub.2023.03.073.

86. Bertolero, M.A., Dworkin, J.D., David, S.U., Lloreda, C.L., Srivastava, P., Stiso, J., Zhou, D., Dzirasa, K., Fair, D.A., Kaczkurkin, A.N., et al. (2020). Racial and ethnic imbalance in neuroscience reference lists and intersections with gender. Preprint at BiorXiv. https://doi.org/10.1101/2020.10.12.336230.

87. Dworkin, J., Zurn, P., and Bassett, D.S. (2020). (In)citing Action to Realize an Equitable Future. Neuron *106*, 890–894. https://doi.org/10.1016/j.neuron.2020.05.011.

88. Llorens, A., Tzovara, A., Bellier, L., Bhaya-Grossman, I., Bidet-Caulet, A., Chang, W.K., Cross, Z.R., Dominguez-Faus, R., Flinker, A., Fonken, Y., et al. (2021). Gender bias in academia: A lifetime problem that needs solutions. Neuron *109*, 2047–2074. https://doi.org/10.1016/j.neuron.2021.06.002.

89. Oostenveld, R., Fries, P., Maris, E., and Schoffelen, J.-M. (2010). FieldTrip: open source software for advanced analysis of MEG, EEG, and invasive electrophysiological data. Comput. Intell. Neurosci. *2011*, 156869. https://doi.org/10.1155/2011/156869.

90. Stolk, A., Griffin, S., van der Meij, R., Dewar, C., Saez, I., Lin, J.J., Piantoni, G., Schoffelen, J.-M., Knight, R.T., and Oostenveld, R. (2018). Integrated analysis of anatomical and electrophysiological human intracranial data. Nat. Protoc. *13*, 1699–1723. https://doi.org/10.1038/s41596-018-0009-6.

91. Monsell, S. (1978). Recency, immediate recognition memory, and reaction time. Cognit. Psychol. *10*, 465–501. https://doi.org/10.1016/0010-0285(78)90008-7.

92. Sternberg, S. (1966). High-Speed Scanning in Human Memory. Science *153*, 652–654. https://doi.org/10.1126/science.153.3736.652.

93. Llorens, A., Funderud, I., Blenkmann, A.O., Lubell, J., Foldal, M., Leske, S., Huster, R., Meling, T.R., Knight, R.T., Solbakk, A.-K., and Endestad, T. (2019). Preservation of Interference Effects in Working Memory After Orbitofrontal Damage. Front. Hum. Neurosci. *13*, 445.

94. McCarty, M.J., Woolnough, O., Mosher, J.C., Seymour, J., and Tandon, N. (2022). The Listening Zone of Human Electrocorticographic Field Potential Recordings. eNeuro *9*. https://doi.org/10.1523/ENEURO.0492-21.2022.

95. Shirhatti, V., Borthakur, A., and Ray, S. (2016). Effect of Reference Scheme on Power and Phase of the Local Field Potential. Neural Comput. *28*, 882–913. https://doi.org/10.1162/NECO_a_00827.

96. Trongnetrpunya, A., Nandi, B., Kang, D., Kocsis, B., Schroeder, C.E., and Ding, M. (2015). Assessing Granger Causality in Electrophysiological Data: Removing the Adverse Effects of Common Signals via Bipolar Derivations. Front. Syst. Neurosci. *9*, 189.

97. Cohen, M.X. (2014). Analyzing Neural Time Series Data: Theory and Practice (MIT Press).

98. Luck, S.J. (2014). An Introduction to the Event-Related Potential Technique, second edition (MIT Press).

99. Jain, A.K. (2010). Data clustering: 50 years beyond K-means. Pattern Recogn. Lett. *31*, 651–666. https://doi.org/10.1016/j.patrec.2009.09.011.

100. Dalmaijer, E.S., Nord, C.L., and Astle, D.E. (2022). Statistical power for cluster analysis. BMC Bioinf. *23*, 205. https://doi.org/10.1186/s12859-022-04675-1.

STAR★METHODS

KEY RESOURCES TABLE

REAGENT or RESOURCE	SOURCE	IDENTIFIER
Deposited data		
Preprocessed data	This paper	https://zenodo.org/record/7995632
All the code for data analysis	This paper	https://github.com/ludovicbellier/InsulaWM
Software and algorithms		
MATLAB 2021a	MathWorks	https://www.mathworks.com/

RESOURCE AVAILABILITY

Lead contact

Further information and requests for resources should be directed to and will be fulfilled by the lead contact, Anaïs Llorens (anaisllorens@hotmail.com).

Materials availability

This study did not generate new materials.

Data and code availability

- The datasets analyzed during this study have been deposited at ZENODO: https://zenodo.org/record/7995632.
- All original code has been deposited at GitHub: https://github.com/ludovicbellier/InsulaWM. The datasets and the code are publicly available as of the date of publications.
- Any additional information required to reanalyze the data reported in this paper is available from the lead contact upon request.

EXPERIMENTAL MODEL AND STUDY PARTICIPANT DETAILS

Human participants

Fourteen patients (4 women, mean age 32.2 years old ± 11.1 SD; 12 right-handed) with epilepsy undergoing stereotactic electroencephalography (SEEG) for pre-surgical investigation at University of California Irvine (UCI; 2) and University of Oslo (OUH; 12) performed the task. The inclusion criterion was the presence of electrodes located in the insula; 3 patients had bilateral implantation, 8 had a right implantation and 3 had a left one, for a total of 90 electrodes. All patients had an IQ score above 80. Two patients, with 2 insular channels each, were removed from the study due to epileptic activity recorded from this region, resulting in 12 participants. The insula of the remaining 12 patients was sampled using electrodes implanted orthogonally (6) or with a combination of oblique (or vertical) and orthogonal electrodes (6). Prior to participation, each patient provided written informed consent as part of the research protocol approved by the Institutional Review Board at every site and by the Committee for Protection of Human Subjects at the University of California, Berkeley, and in accordance with the Declaration of Helsinki. The study was also approved by the Regional Committees for Medical and Health Research Ethics of Norway.

METHOD DETAILS

Electrode localization

The electrodes were localized for each subject based on their individual anatomy and then transferred into the standard MNI space for representation. Affine point-based registration was used to co-register post-implantation computed tomography (CT) images to the pre-implantation magnetic resonance (MR) images using the FieldTrip toolbox[89,90] in MATLAB (MathWorks, Inc., Natick, MA, USA). The anatomical location of each electrode on patients' individual anatomy was confirmed by a neurologist (RTK).

3D insula model reconstruction

To reconstruct the fine-grained 3D anatomy of the insulae, we extracted surfaces of both insulae from the MNI template brain MRI with a parcellation based on the Desikan-Killiany Atlas (aparc+aseg), using iso2mesh with 3000 vertices and 10 smoothing steps. We then manually corrected spurious vertices using a custom GUI created in MATLAB and delineated insular subregions based on two previous studies[34,35] (Figure 2B). Finally, we snapped all electrodes onto the insular mesh at the closest vertex (Euclidean distance) of the lateral insular face (Figure 2A).

Experimental task and setup

The experimental paradigm was a Recent-Probes task[91,92] (Figure 1A). Each trial was composed of a list of five letters displayed on the screen for 500ms each, with an interstimulus interval of 500ms. This encoding phase was followed by a 3.5-second period of maintenance (represented by a cross on the screen). A question was then displayed for 2s asking whether a given letter, i.e., the probe, was in the current list. The probe letter was present in the current list for half of the trials (positive condition) and absent from it for the other half (negative condition). The task included a total of 144 trials in pseudorandomized order for each participant. The trials were presented in three blocks of 10 min each, with short breaks between blocks, resulting in a total study duration of approximately 35 min.

The participants were seated on their hospital bed, with the laptop placed in front of them on an overbed table. A photodiode was placed on the bottom left corner of the laptop screen and recorded as a channel (UCI), or alternatively a digital trigger (TTL) was used to mark each timestamp of interest (OUH).

The instructions were displayed on the screen and required the participants to respond "yes" (positive response condition) or "no" (negative response condition) by pressing the mouse keys using their index and middle finger, respectively. No feedback was provided. To prevent potential interference of motor activity due to button presses occurring simultaneously with the electrophysiological signals of interest, the hand used for the task was ipsilateral to the implantation when the implantation was unilateral. For bilateral implantations, one participant used their right hand while the two other participants used their left hand.

Behavioral analysis

The response time at the probe was recorded for each trial. Trials with RT faster than 400ms[92] or exceeding three standard deviations were excluded.[93] The remaining trials were included in subsequent analyses of response latency (based on the mean RT of correct trials per participant) and error rate (based on the percentage of incorrect trials). We performed Wilcoxon signed-rank tests in MATLAB to test the hypothesis of similar mean RT between positive and negative answers for correct trials, and to assess a potential difference in error rate between positive and negative answers.

SEEG data acquisition and preprocessing

Two datasets were acquired at UCI using a Nihon Kohden recording system (Nihon Kohden Corporation, Japan) sampling at 5kHz. The 10 other datasets were recorded at OUH: 4 datasets were acquired using a NicoletOne system (Nicolet, Natus Neurology Inc., USA), 1 dataset using a 256-channel Brain Quick system (Micromed, Italy), and 5 with an ATLAS system (Neuralynx, USA). The sampling rates were 512Hz, 2048Hz, and 16kHz respectively. Each SEEG shaft was composed of 5 to 18 electrodes spaced 5mm apart for UCI (Ad-Tech, Racine, WI, USA) and 3.5mm apart for OUH (DIXI Medical, France).

Raw data with a sampling rate higher than 1kHz was downsampled offline to 1kHz and filtered with 1Hz high-pass and 250Hz low-pass filter (4th order Butterworth). In addition, 60Hz for UCI and 50Hz for OUH power-line noise frequency and harmonics were removed using notch filters. The filtered data was then visually inspected under the supervision of a neurologist (RTK) to identify and discard from further analyses channels and epochs displaying epileptiform activity or artifactual signals (from poor or broken contact, machine noise, etc.). Clean, artifact-free, continuous data was epoched into 16s-long trials (from -11.5 to 4s, 0s being the probe presentation; epochs included 2s of data padding at each extremity to avoid edge artifacts in the following time-frequency (TF) decomposition).

Each trial encompassed the encoding of the five successively presented letters (from 8.5 to 3.5s before the probe presentation), the maintenance of the letters (3.5s leading up to the probe presentation at 0s), and the probe period (from 0 to 2s post-probe onset). Behavioral information of each trial (condition, RT, and accuracy) was preserved during the epoching. The epoched data was re-referenced using bipolar montage (i.e., subtraction of the activity of a given electrode from the previous neighbor electrode on the same SEEG shaft,[62] yielding 96 virtual channels with minimized contamination from volume conduction.[94–96] A visual re-inspection of the bipolar data was performed to reject any remaining channels or epochs containing residual artifacts, resulting in the removal of six insular channels. The complete preprocessing yielded a total of 90 artifact-free bipolar channels (with at least one electrode in the insula for each channel). All preprocessing steps and subsequent analyses were performed using the FieldTrip toolbox for MATLAB and custom MATLAB scripts.

We performed a TF decomposition of all correct trials using Morlet wavelets, over a frequency range from 4 to 150Hz (logarithmically spaced in 32 steps) and using a time resolution of 5ms resulting in a sampling rate of 200Hz. The wavelet order (width or number of cycles) was logarithmically increased from 4 to 30 cycles (also in 32 steps). A baseline correction (with the second preceding the encoding onset used as baseline period) was then applied using the decibel method.[97] Lastly, the padding time periods were removed so that the remaining epochs lasted 11.5s (-9.5 to 2s relative to the probe presentation).

QUANTIFICATION AND STATISTICAL ANALYSIS

Analyses over the entire vWM process

We first extracted the time courses of the 3 frequency bands of interest (theta: 4-8Hz; beta: 13-30Hz; High-Frequency Activity, or HFA: 70-150Hz), by averaging the corresponding baseline-corrected frequency bins of the TF decomposition.

We then fitted a linear mixed-effects model on the frequency band envelopes of the 90 channels using the fitlme MATLAB function. The anatomical locations (right/left and anterior/posterior), the three time periods (encoding, maintenance and probe) and the three time-frequency bands (theta, beta, HFA) were used as fixed effects while the patients and the electrodes were used as random effects. The main

effects were assessed for significance by computing an ANOVA on the model and the post-hoc tests were performed using the coefTest MATLAB function with an alpha value Bonferroni-corrected by the number of post-hoc tests (3 levels for frequency bands and 3 levels for time periods, for a total of 6 tests).

For each frequency band and each channel, we computed a paired-sample t-test comparing each time sample contained in the trial (-8.5 to 2s) against the baseline mean (-9.5 to -8.5s). We then isolated the significant time samples that stayed significant (p<.05) for at least 25 consecutive ms using a Bonferroni correction to compensate for multiple comparisons (alpha value divided by the number of time samples) and labeled the channel as responsive. Frequency modulations were considered significant if at least 2 responsive channels were significant for the same time sample, regardless of the patient (see Figure S1).

Analyses at the probe period

Similar parameters (i.e., p<.05, 25 consecutive ms) as for the entire time window were used to extract the frequency band time courses at the probe period (0 to 2s]). The paired sample t-tests to select the responsive channels were computed against the mean of the second preceding the probe onset (-1 0s).

We assessed the difference of frequency band modulation latencies between the anterior and posterior parts of the insula by using the fractional area method.[98] For each frequency band and each responsive channel, we first set the minimum of the time course to zero and normalized it between 0 and 100%. We then computed the cumulative area under the curve (AUC) over the time window of interest (0 to 2s). The time point separating the cumulative AUC in two equal parts (50%) was extracted. A Wilcoxon rank sum test was performed to assess latency differences between anterior and posterior insular channels. A Bonferroni correction was performed to compensate for multiple comparisons by dividing the alpha value by the number of tests (6).

For each responsive channel, correct trials were sorted by ascending RT and then grouped into 10 bins of trials equitably distributed across bins (for denoising purposes). Note that due to varying numbers of correct trials across patients, the tenth bin sometimes contained less trials than the nine other bins. We then extracted the mean RT and the mean temporal profile of each bin of the probe time window (0 to 2s), resulting in a 10-by-400 matrix (2s epoch at a 200Hz sampling rate).

We then performed a k-means analysis to cluster these RT-sorted temporal profile matrices, based on the nearest centroid using the Squared Euclidean distance.[99,100] For each of the 3 frequency bands of interest, we evaluated the optimal number of clusters using the Calinski-Harabasz clustering evaluation criterion, replicated 500 times. This optimal number analysis revealed the presence of two main clusters for each frequency band. We then visualized cluster centroids and plotted the channels of each cluster on both insulae.

We compared the spatial distribution of the channels within the k-means clusters obtained for each frequency band by performing Fisher's exact tests. For each frequency band, we compared antero-posterior and inter-hemispheric distributions of channels across clusters.

Correlation with behavioral response time

For each frequency band and for each cluster, we performed linear correlations between the peak (or trough) of activity of the cluster centroids, i.e., the latency of the maximum (or minimum) value of each of the 10 sub-averaged temporal-profile bins, and the mean RT. A Bonferroni correction was performed to compensate for multiple comparisons by dividing the alpha value by the number of correlations (number of clusters by number of frequency bands).